Nanoscale

RSC Publishing

PAPER

View Article Online
View Journal | View Issue

Inverted CdSe/CdS/ZnS quantum dot light emitting devices with titanium dioxide as an electron-injection contact

Cite this: *Nanoscale*, 2013, **5**, 3474

Wenyu Ji,[a] Pengtao Jing,[a] Jialong Zhao,*[ab] Xingyuan Liu,[a] Andrew Wang[c] and Haibo Li*[b]

We demonstrated the fabrication of inverted CdSe/CdS/ZnS quantum dot light emitting devices (QD-LEDs) using titanium dioxide (TiO_2) as an electron-injection layer and investigated the operating mechanism by utilizing different hole-transport materials, 4,4-*N*,*N*-dicarbazole-biphenyl (CBP) and 4,4′,4″-tris(carbazol-9-yl)-triphenylamine (TCTA). A more efficient device with CBP as the hole-transport layer (HTL) was obtained compared with the TCTA based device. The peak efficiency of 6.70 cd A^{-1} for the CBP based device was found to be about 74.5% higher than the TCTA based device (3.84 cd A^{-1}). The studies on the time-resolved photoluminescence spectra of the QD–HTL composite structures showed that the energy transfer (ET) efficiencies from the two HTLs to the QD layer were similar and the charge separation between QDs and HTLs could be neglected. The enhancement in the performance of the CBP based device was attributed to the more efficient hole-injection from CBP to QDs.

Received 18th December 2012
Accepted 25th February 2013

DOI: 10.1039/c3nr34168b

www.rsc.org/nanoscale

1 Introduction

Semiconductor quantum dots (QDs) have been widely studied for their potential applications in full-color flat-panel displays (FPDs) due to their unique optoelectronic properties and high emission quantum yield (QY), which can be tuned by changing their size and components.[1–9] QDs based light emitting devices (QD-LEDs) possess promising features of a much wider color gamut than current FPDs,[10] such as liquid crystal displays and organic LEDs, due to the narrow emission (full width at half-maximum (FWHM) < 30 nm) of monodisperse QDs as well as their tunable emissions in the full visible spectral range. Moreover, these QDs can be solved in common solvents enabling solution processing, which is low cost and has been widely used in the development of optoelectronic devices. Although the use of QDs in solution-processed QD-LEDs is promising, a serious drawback still exists in present technology. To date, the most conventional QD-LEDs reported in the visible region are the hybrid QD–organic devices composed of a monolayer (ML)/multilayer of closely packed CdSe/ZnS core–shell QDs sandwiched between electron and hole-transport layers (HTLs) and the most commonly used hole-transport material is organic poly[bis(4-butylphenyl)-bis(phenyl)benzidine] (poly-TPD).[8,9,11,12] This HTL is solvent-sensitive and in order to achieve a multilayer structure device using a solution process we must use the orthogonal solvents to avoid compromising the integrity of the underlying layers while depositing overlayers, which limits the choice of the hole-injection and transport materials. In addition, even though we use the orthogonal solvents, it is still unavoidable to damage the organic underlayer during QD deposition, which can degrade the performances of QD-LEDs.

As we know, two mechanisms have been proposed to explain electroluminescence (EL) of QD-LEDs.[13–15] For the first one, carriers transported through organic charge-transport layers are directly injected into QDs, where they can form excitons that then can radiatively recombine. The second one depends on the ability to form excitons on the organic molecules surrounding the QD film that then resonantly transfer the exciton energy to QDs. Here, we define the first mechanism as the charge-injection (CI) type (*i.e.* CI-type) and the second one as the energy-transfer (ET) type (*i.e.* ET-type). In a conventional QD-LED, the barrier to hole-injection between the HTL (*e.g.* poly-TPD) and QDs is much larger (more than 1 eV) than that of electron-injection from the electron-transport layer to the QD, because the QDs intrinsically exhibit lower valence band (VB) (∼−6 to −7 eV) and conduction band (CB) (∼−4 eV) energy levels as compared with the highest occupied molecular orbital (HOMO) and the lowest unoccupied molecular orbital (LUMO) energy levels of typical conjugated organic molecules or polymers (about −5.5 and −3 eV, respectively). As a result, excitons are formed at the HTL–QDs interface. Consequently, the selection

[a]*State Key Laboratory of Luminescence and Applications, Changchun Institute of Optics, Fine Mechanics and Physics, Chinese Academy of Sciences, Changchun 130033, China. E-mail: zhaojl@ciomp.ac.cn; Tel: +86-431-86176313*

[b]*Key Laboratory of Functional Materials Physics and Chemistry of the Ministry of Education, Jilin Normal University, Siping 136000, China. E-mail: lihaibo@jlnu.edu.cn*

[c]*Ocean NanoTech, LLC 2143 Worth Lane, Springdale, Arkansas 72764, USA*

of hole-injection materials becomes more important no matter which mechanism is implemented in QD-LEDs. Unfortunately, due to this drawback of present fabrication technology for conventional QD-LEDs discussed above, introducing an appropriate HTL into the QD-LEDs is limited, which requires more complicated stamping deposition techniques.[16] In spite of this, it is highly desirable to explore the operating mechanism and improve the performance of the QD-LEDs by introducing suitable HTL materials. A wise device structure enabling the choice of hole-injection materials flexibly is still a challenge.

In this work, we demonstrate successful fabrication of an inverted CdSe/CdS/ZnS QD-LED structure. The devices reported herein operate in a reverse manner to conventional QD-LEDs in that the ITO/TiO_2 electrode serves as the electron-injecting cathode and the Al metal electrode serves as the anode. The TiO_2 film is mechanically smooth and amorphous in composition, which prevents electrical shorts or the formation of preferred current channels through the device structure. Because the TiO_2 layer can be annealed at low temperature (<150 °C), it is neither in a crystalline phase nor fully inorganic, which results in the formation of a TiO_2 layer having a moderate carrier mobility of 1.7×10^{-4} cm^2 V^{-1} s^{-1}.[17] The low free-carrier concentration TiO_2 film will minimize quenching of the QD EL through free-carrier plasmon modes.[18] Different HTLs are tested in our experiments, and the results reveal that the CI-type plays a dominating role in the inverted QD-LEDs. For the CI-type mechanism, carriers must be injected into the QDs from the charge-transport layers neighboring the QD layer. A high barrier between the HTL and QD layer will reduce the device efficiency. Hence, the HTL applied should be carefully selected on the basis of the energy level of the HOMO. With CBP as the HTL, the QD-LED shows higher current efficiency than the TCTA based one. This inverted structure paves the way for developing QD-LEDs *via* a new method with a very flexible choice of HTL materials and increases the potential to improve the device efficiency.[19]

2 Experimental

The red CdSe/CdS/ZnS core–shell QDs were synthesized with a method in previous reports.[17] The room temperature absorption spectrum was measured by means of a ultraviolet/visible spectrometer (UV 1700, Shimadzu). The photoluminescence (PL) spectrum of the QDs in toluene was collected by a Hitachi F-4500 spectrophotometer under an excitation wavelength of 480 nm. The fluorescent QY of the QDs prepared was measured and estimated by comparing their fluorescence intensities with those of primary standard dye solutions (with emission close to the QDs) at the same optical density (0.06) at the same excitation wavelength. The QY of our QD sample was estimated to be ~60%. The crucial step in QD-LED design is the choice of HTL that surrounds the luminescent centers of QDs. In our QD-LEDs, we chose organic hole-transport materials, CBP and TCTA as the HTLs.

The QD-LEDs consisted of glass/ITO/TiO_2 (35 nm)/QDs (~3 MLs)/HTL (45 nm)/MoO_3 (8 nm)/Al (200 nm). The ITO glass substrates were cleaned in an ultrasonic bath with isopropyl alcohol, acetone, and methanol sequentially. A TiO_2 sol–gel precursor (DuPont tyzol BTP) was diluted to 7 wt% in butanol for spin-coating as the ETL. Spin-coating was performed at 2500 rpm for 60 s and then subsequently annealed at 110 °C for 30 min in glove box (MBRAUN) and naturally cooled to room temperature. After that, QDs dissolved in toluene (the optical density (OD) of the QD solution was 3.2 at a wavelength of 616 nm, which was estimated from the diluted solution) were deposited by spin-coating at 1200 rpm for 60 s, followed by drying in a glove box (MBRAUN) at 70 °C for 30 min. Then, organic hole-transport materials (CBP for device A and TCTA for device B), MoO_3, and Al were successively deposited by thermal evaporation at a pressure below 4×10^{-6} Torr. The layer thickness and the deposition rate of the materials were monitored *in situ* using an oscillating quartz thickness monitor. The deposition rates of organic materials, MoO_3, and Al were controlled to 0.2, 0.05, and 0.5 nm s^{-1}, respectively. The characteristics of current–voltage–luminance and EL spectra were measured by a programmable Keithley model 2400 power supply and a Minolta Luminance Meter LS-110, respectively, in air at room temperature. For all devices, no external package or encapsulation was applied after device fabrication. The atomic force microscopy (AFM) images were recorded by a Nanosurf EasyScan2 FlexAFM. The morphology of the QD and TiO_2 films was characterized by scanning electron microscope (SEM) (Hitachi S4800). Time-resolved photoluminescence (TRPL) measurements were carried out with a Edinburgh Instruments FL920 spectrometer. For the TRPL measurements, the samples were fabricated on quartz substrates and all the films were fabricated using the same technique described above. The various samples for TRPL measurements are as follows:

S-A: substrate/red QD (~3 ML); S-B: substrate/red QD (~3 ML)/CBP (10 nm); S-C: substrate/red QD (~3 ML)/TCTA (10 nm); S-D: substrate/CBP (10 nm); S-E: substrate/TCTA (10 nm).

3 Results and discussion

Fig. 1a shows the AFM images of bare (left) and a TiO_2 layer coated (right) ITO substrates. As can be seen, a root-mean-square roughness of ~1.9 and 2.2 nm is obtained for bare and TiO_2 coated ITO substrates, respectively. The deposition of TiO_2 on the ITO substrate slightly increases the roughness of the surface. To evaluate the capability of electron-injection from the ITO electrode to the TiO_2 film, an electron-only device with a structure of ITO/TiO_2 (~80 nm)/Al (200 nm) was fabricated firstly. The hole-injection is negative due to the very large barrier from Al or ITO to TiO_2 film. As seen from Fig. 1b, the electron-injection current from the top Al electrode with forward-bias voltage (Al is used as the cathode) is nearly symmetric with that from bottom ITO electrode with reverse-bias voltage (ITO is used as the cathode), indicating that the bottom ITO electrode is comparable to the top Al electrode at injecting electrons into the TiO_2 layer. Fig. 2 shows the SEM image of the QD layer on TiO_2 with a silicon substrate. The inset is the SEM (Hitachi S4800) image of TiO_2 on silicon substrate. As can be seen, a high quality close-packed QD film is obtained. In fact, the QD layer is

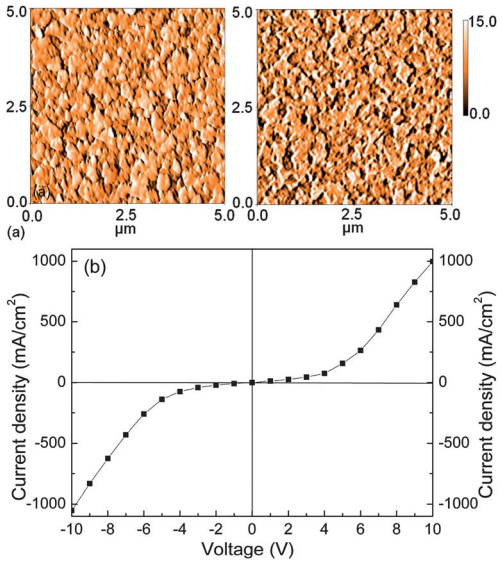

Fig. 1 (a) AFM images of bare (left) and TiO_2 layer coated ITO substrates (right); (b) the current density–voltage curve for the electron-injection only device.

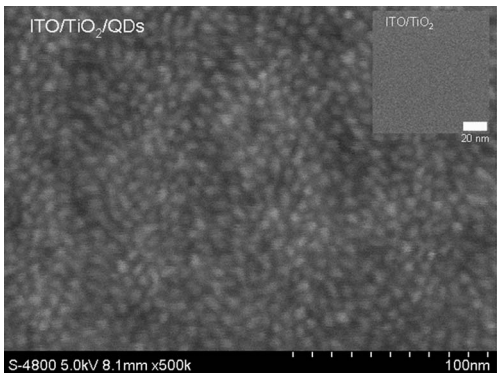

Fig. 2 The SEM image of the CdSe layer on TiO_2 film with a silicon substrate. The inset shows the SEM image of the TiO_2 film on silicon substrate.

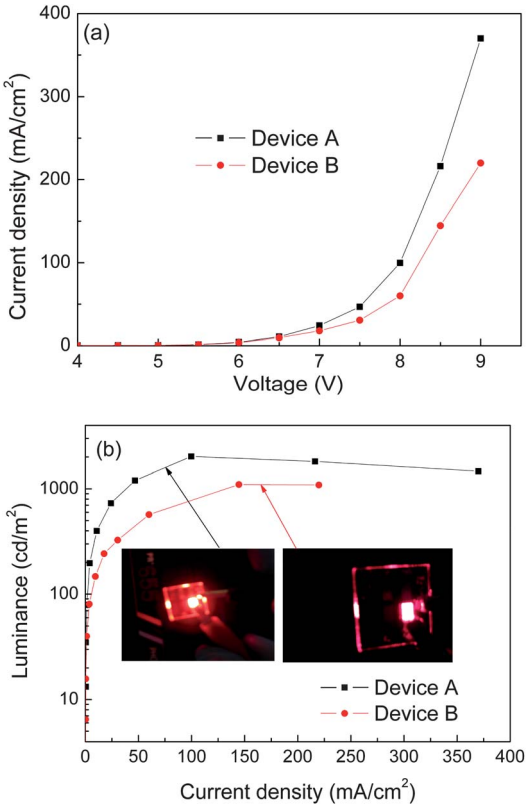

Fig. 3 (a) The current density–voltage and (b) luminance–voltage characteristics of CdSe/CdS/ZnS QD-LEDs.

not always perfect. Some streaks of imperfections, voids, and grain boundaries were observed. The work for the preparation of a very smooth QD layer on TiO_2 is currently under investigation.

The current density–voltage and luminance–voltage characteristics of CdSe/CdS/ZnS QD-LEDs with various HTLs are plotted in Fig. 3a and b. This clearly shows their difference in driving voltages, brightness, and turn-on voltages due to the different energy barrier between QDs and each HTL. For instance, when the current density is 100 mA cm^{-2}, the driving voltages are 8.0 and 8.2 V and the luminance is 2031 and 810 cd m^{-2} for devices A and B, respectively. In other words, the performance of device A, including the driving voltage lowered by 2.3% and the luminance enhanced by 151%, is significantly improved at the same current density of 100 mA cm^{-2} relative to device B.

Fig. 4a shows the current efficiency–voltage characteristics of CdSe/CdS/ZnS QD-LEDs. We can see that a higher efficiency can be achieved with CBP as the HTL, which is in agreement with that discussed above. The peak efficiency of 6.70 cd A^{-1} is achieved for device A at a driving voltage of 5.0 V, around 74.5% higher than the maximum efficiency of device B, 3.84 cd A^{-1} at a driving voltage of 5.0 V. We consider that the significantly improved performances result from the direct and efficient carrier recombination within QD layers owing to the facilitated charge carrier-injection into QDs from TiO_2 and CBP or TCTA. Fig. 4b shows the EL spectra of devices A and B measured at a voltage of 7.0 V. The PL and absorption spectra of CdSe/CdS/ZnS QDs in toluene are also shown in Fig. 4b. The narrow FWHM and excitonic peak indicate that our QD sample has a narrow size distribution and high quality. As seen from Fig. 4b, the two devices have the same EL spectra, which indicates that the variety of HTL does not change the feature of the devices and the recombination range is still on the QD layer. The FWHM of the EL for the QD-LEDs demonstrated herein is 28.9 nm. The peak wavelengths of the observed EL spectra are slightly red shifted compared to the PL spectrum. It is likely that the shift is due to the Förster resonant energy transfer (FRET) from smaller (donor) to larger (acceptor) dots within the film. Also, the low-energy region of the EL spectrum does not exhibit any feature emission at any current density–voltages,[20] demonstrating the absence of emission from deep-level trap states and adjacent hole-transport materials. Furthermore, there is no parasitic emission in the high-energy region of the EL spectrum from the neighboring organic layers over the entire range of current density (voltages). All the results demonstrate that the excitons

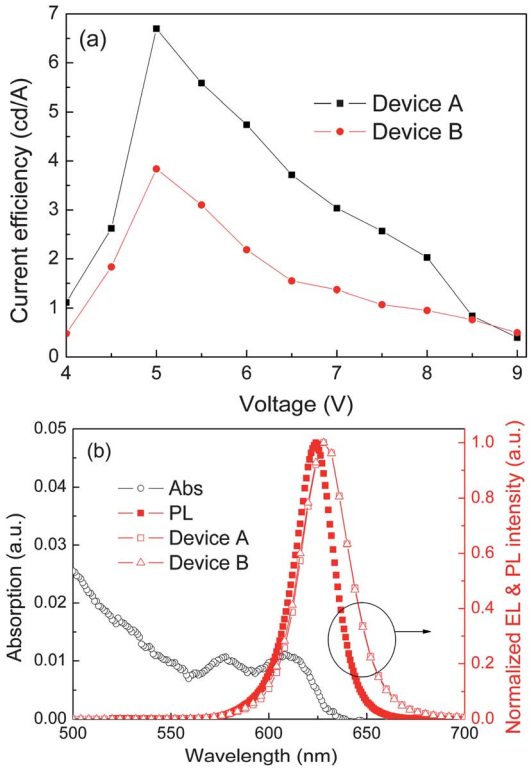

Fig. 4 (a) Current efficiency–voltage curves of devices A and B; (b) EL spectra of devices A and B measured at voltage of 5.0 V and the PL and absorption spectra of CdSe/CdS/ZnS QDs in toluene.

effectively recombine in the QD layer. The inset shows the photograph of the device driving at 5.0 V. The EL of our QD-LED is sufficiently bright and vivid.

The enhancement of the performance for device A is attributed to the utilization of CBP because the two devices have the same structure except for the HTL. As mentioned above, two work mechanisms, CI type and ET type, were proposed in QD-LEDs. It is important to understand which mechanism is dominating in our inverted devices and why the CBP based device has better performance. To determine which of the factors is primarily responsible for the observed enhanced performance, we have studied the energy level alignment and ET efficiency between HTLs and QDs.

Firstly, we investigate the energy level alignment for the materials in our work as depicted in Fig. 5, in which the HOMO, LUMO, VB, and CB levels of the materials are taken from the literature.[19,21–24] As can be seen, the potential energy barrier is 0.7 and 0.4 eV for the hole-injection from TCTA and CBP into the QD, respectively. A lower potential energy barrier to hole-injection from CBP into QDs is benefit to the performance of the QD-LED. Compared with the turn-on voltage of 4.0 V for device B, a much lower turn-on voltage of 3.4 V is obtained for device A owing to the facilitated hole-injection into QDs from CBP.

Then we analyze the FRET process, including the spectral overlap integral between acceptor absorption and donor emission and the Förster radius. The overlap integral J is defined as follows:[25]

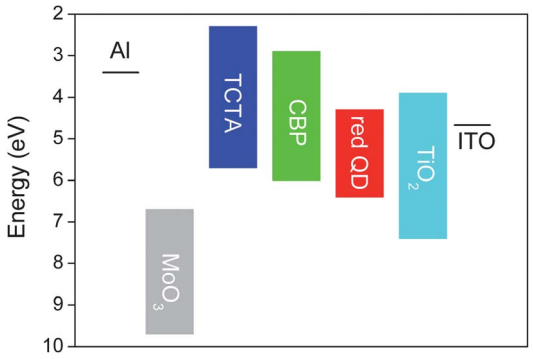

Fig. 5 Energy-level diagram of the materials used in our work.

$$J = \int_0^\infty F_D(\lambda)\varepsilon_A(\lambda)\lambda^4 d\lambda \quad (1)$$

where $F_D(\lambda)$ is the normalized donor emission spectrum and $\varepsilon_A(\lambda)$ is the acceptor molar extinction coefficient. The Förster radius R_0 is defined as the separation distance corresponding to 50% FRET efficiency, which can be expressed as:[25]

$$R_0 = \left(\frac{9000(\ln 10)Q_D\kappa^2}{128\pi^5 N_A n_D{}^4}J\right)^{1/6} \quad (2)$$

where Q_D is the QY of the donor (70% for CBP and 60% for TCTA), N_A is Avogadro's number, n_D refers to the refractive index of the medium and the value of 1.8 is used for organic materials, κ is a parameter that depends on the relative orientation of the donor and acceptor dipoles. We used $\kappa^2 = 2/3$ here for randomly oriented dipoles. The Förster radius R_0 is estimated to be 7.2 and 7.1 nm for TCTA and CBP, respectively. The FRET efficiency, η_{ET}, can be calculated by:[25]

$$\eta_{ET} = \frac{R_0{}^6}{R_0{}^6 + r^4} \quad (3)$$

where r is the distance between the donor (HTL) and acceptor (QDs). In our devices, the distance between HTLs and QD is the same due to the identical fabricating process of TCTA and CBP. Consequently, the FRET efficiency from TCTA to QD should be the same as that from CBP to QD according to eqn (3) due to the similar r and R_0.

Fig. 6a shows the normalized PL spectra of CBP and TCTA. The emission peaks are 372 and 419 nm for CBP and TCTA in chloroform solvent at room temperature, respectively. An effective overlap between the PL spectra of HTLs and the absorption spectrum of the QDs is obtained, which is the prerequisite for FRET.[26] In order to obtain the actual FRET efficiency from HTLs to QDs, we have measured the PL lifetimes of the HTLs, CBP and TCTA, in samples S-B, S-C, S-D, and S-E by measuring the TRPL. The PL decay curves of the CBP in QD–CBP and TCTA in QD–TCTA films are shown in Fig. 6b and c. The PL dynamic signal was collected at 372 and 420 nm for CBP and TCTA, respectively. Fitting the TRPL decay curves by convoluting the instrument response function (IRF) with a two-exponential equation, the average PL lifetimes of neat TCTA

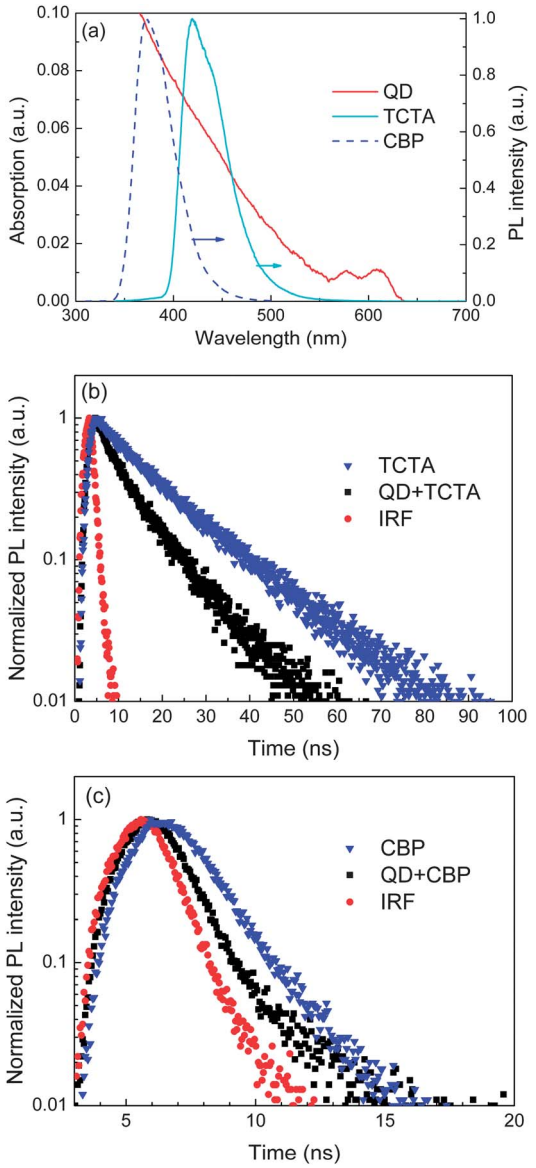

Fig. 6 (a) The PL spectra of TCTA, CBP, and CdSe/CdS/ZnS QDs and absorption spectrum of the QDs in toluene; the PL decay curves of the CBP in QD–CBP (b) and TCTA in QD–TCTA films (c).

(τ_{TCTA}) and CBP (τ_{CBP}) are determined to be 16.86 and 1.21 ns, respectively. The PL lifetime of TCTA in sample S-C ($\tau_{TCTA+QD}$) and CBP in sample of S-B (τ_{CBP+QD}) is 10.94 and 0.76 ns, respectively. The ET efficiency ($\eta_{ET} = 1 - \tau_{HTL+QD}/\tau_{HTL}$, τ_{HTL} and τ_{HTL+QD} is the PL lifetime of HTL in S-B/S-C and S-D/S-E, respectively) is calculated to be 35% and 37% for TCTA and CBP, respectively.[25] The efficiencies of the FRET are similar for the two HTLs to QDs, which eliminates the effect of FRET on the difference between the performance of the two devices. The better performance of device A is mainly attributed to the direct and efficient exciton recombination within the QD layer through the CBP based device structure.[19] As discussed above, the CBP only improves the hole-injection into the QD layer and has no effect on the ET from HTL to QD layer, which indicates the enhanced performance of device A is due to the more efficient hole-injection from CBP to QDs. Thus, CI-type must be the dominating work mechanism. Further, the EL spectra of the two devices are only from the QDs, no emission from HTL is observed, which also indicates that the possibility of excitons on the HTL is very low. If this is not the case, the emission from the HTL should be observed due to the low ET efficiency from HTLs to the QD layer.

However, it is valuable to note a type II aligned structure may induce the charge separation between QDs and adjacent organic materials. The charge transfer from QDs to HTL will lead to a reduced efficiency of the QD-LEDs. In order to further understand the operating mechanism of the QD-LEDs based on TCTA and CBP as the HTLs, we have measured the TRPL of QDs in the samples S-A, S-B and S-C. The PL decay curves of the pure QD, QD–CBP, and QD–TCTA films are shown in Fig. 7. The QD–HTL composite structures were excited at wavelength of 480 nm and the emission of the QDs was collected at the wavelength of 624 nm (the peak wavelength of QD layer). The excitation wavelength was selected below the absorption edge of CBP and TCTA molecules avoiding the contribution of ET from CBP to the QDs. Three samples have identical values within the error margin of our measurements, and the PL lifetimes of the QD, QD–TCTA, and QD–CBP are determined to be 12.3, 12.9, and 12.8 ns, respectively, which demonstrates a neglectable charge separation from QDs to HTLs, TCTA and CBP. Here, we can eliminate the possibility that the lower efficiency of the TCTA based device is due to the charge separation from QDs to TCTA, which possesses a higher energy offset. In response what is discussed above, we can draw the conclusion that the direct charge-injection is the dominating mechanism in the inverted CdSe/CdS/ZnS QD-LEDs and the worse performance of the TCTA based device is ascribed to the higher injection barrier from TCTA to QDs rather than the charge separation between TCTA and QDs. Therefore, suitable material choices for HTLs can enhance the hole-injection efficiency and improve the device performance.

The Commission Internationale de l'Enclairage (CIE) coordinates of the emitted lights of the both QD-LEDs are (0.70, 0.30) as depicted in Fig. 8. When the CIE coordinates of the QD-LEDs are compared with the colour triangle of the National

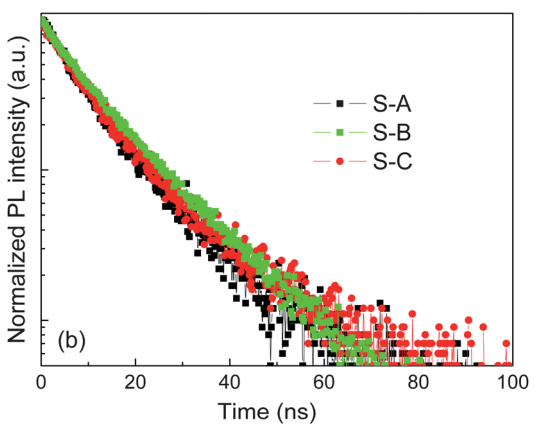

Fig. 7 The PL decay curves of the pure QD, QD–CBP, and QD–TCTA films.

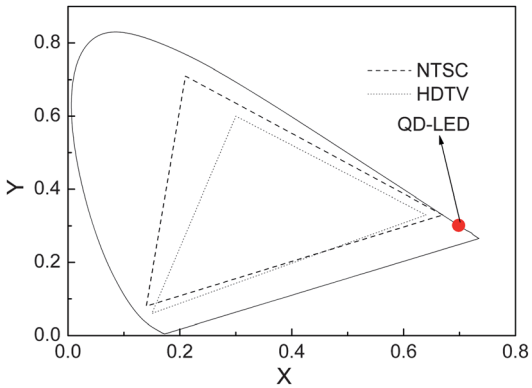

Fig. 8 The CIE coordinates of the emitted lights of both CdSe/CdS/ZnS QD-LEDs with TCTA and CBP as the HTLs.

Television System Committee (NTSC) 1953, the QD-LED color is in excess of the high-definition-television (HDTV) standard[27] without additional optical outcoupling techniques.

Fig. 9 shows the comparison of operation times for QD-LEDs with standard and inverted structures. The measurement was carried out in air at room temperature and without any external package or encapsulation for the devices. The QD-LED with the standard device structure consisting of ITO/PEDOT:PSS (20 nm)/poly-TPD (30 nm)/QDs/1,3,5-tris(*N*-phenylbenzimidazol-2-yl)benzene (TPBI, 45 nm)/LiF (0.5 nm)/Al (200 nm) shows rapid deterioration within tens of minutes of continuous operation at a constant current density corresponding to an initial luminance of 100 cd m^{-2}. In contrast, QD-LEDs with an inverted structure (device A) exhibit better device stability, which is in agreement with the result reported in ref. 19.

Although the device performance, especially for the luminance, is inferior to that reported in ref. 19, the current efficiency of our device (6.7 cd A^{-1}) is similar to that in ref. 19 (5.7 cd A^{-1}). The most important work here is that we focus on the study of the EL mechanism in the QD-LEDs. Our results provide a clear route for further improvement of LED performances. We note here that these devices have not been well optimized, so more efficient QD-LEDs would be expected after optimization of the device parameters and QD samples. Furthermore, we believe that we have not yet reached the limit of device optimization because we speculate that a large fraction of the injected current is shunted through the device due to the roughness of the TiO_2 surface. The deposition of a sol–gel TiO_2 layer deteriorates the surface morphology of the ITO substrate (the RMS is changed from 1.9 to 2.2 nm). A much rougher surface of TiO_2 coated substrate will lead to a higher leak current in the devices. We expect to improve the efficiency of the QD-LEDs with a smoother TiO_2 surface, due to the reduction of shunt currents from direct contacts between TiO_2 spikes and the CBP layer.

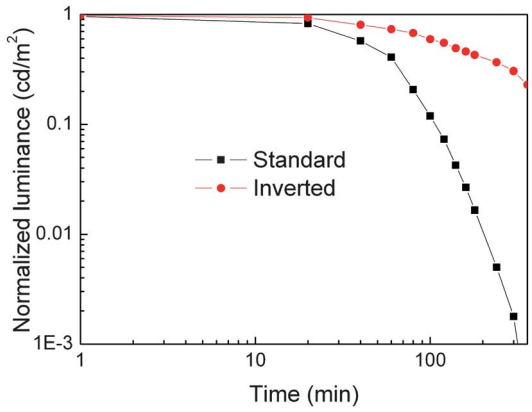

Fig. 9 The operational lifetime characteristics of QD-LEDs with standard and inverted structure.

4 Conclusions

In conclusion, inverted CdSe/CdS/ZnS QD-LEDs with different HTLs have been successfully fabricated. A better performance (higher luminance and current efficiency, lower turn-on voltage) of the CBP based QD-LED was obtained compared with the TCTA based device. The operating mechanism of the TCTA and CBP based inverted QD-LEDs was understood in terms of dominant direct charge-injection by measuring the TRPL spectroscopy of QDs–HTL hybrid systems and EL spectra of the devices. Especially, the use of a stable inorganic material, TiO_2, as the robust electron-injection layer enables deposition of QDs by spin-coating or even inkjet-printing out of organic solutions. This is in contrast to solvent-sensitive organic thin films, which require more complicated stamping deposition techniques.[16] In addition, this structure of inverted QD-LEDs enables the systematic engineering of HTLs built by evaporation deposition with conventional organic materials with proven performances. Consequently, the introduction of metal oxides has expanded and simplified the fabrication process of QD-LEDs.

Acknowledgements

This research was supported by the program of CAS Hundred Talents and the National Natural Science Foundation of China (no. 61205025, 11274304, and 11204298).

Notes and references

1 L. E. Brus, *J. Chem. Phys.*, 1984, **80**, 4403–4409.
2 V. L. Colvin, M. C. Schlamp and A. P. Alivisatos, *Nature*, 1994, **370**, 354–357.
3 Y. Masumoto and K. Sonobe, *Phys. Rev. B: Condens. Matter*, 1997, **56**, 9734–9737.
4 M. Drndić, M. V. Jarosz, N. Y. Morgan, M. A. Kastner and M. G. Bawendi, *J. Appl. Phys.*, 2002, **92**, 7498–7503.
5 J. Zhao, J. Bardecker, A. Munro, M. Liu, Y. Niu, I. Ding, J. Luo, B. Chen, A. Jen and D. Ginger, *Nano Lett.*, 2006, **6**, 463–467.
6 D. V. Talapin, J. Lee, M. V. Kovalenko and E. V. Shevchenko, *Chem. Rev.*, 2010, **110**, 389–458.
7 W. K. Bae, J. Kwak, J. W. Park, K. Char, C. Lee and S. Lee, *Adv. Mater.*, 2009, **21**, 1690–1694.

8 Z. Tan, F. Zhang, T. Zhu, J. Xu, A. Y. Wang, J. D. Dixon, L. Li, Q. Zhang, S. E. Mohney and J. Ruzyllo, *Nano Lett.*, 2007, **7**, 3803–3807.
9 Q. Sun, Y. A. Wang, L. S. Li, D. Wang, T. Zhu, J. Xu, C. Yang and Y. Li, *Nat. Photonics*, 2007, **1**, 717–722.
10 A. Rizzo, Y. Li, S. Kudera, F. D. Sala, M. Zanella, W. J. Parak, R. Cingolani, L. Manna and G. Gigli, *Appl. Phys. Lett.*, 2007, **90**, 051106.
11 L. Qian, Y. Zheng, J. Xue and P. H. Holloway, *Nat. Photonics*, 2011, **5**, 543–548.
12 W. K. Bae, J. Kwak, J. Lim, D. Lee, M. K. Nam, K. Char, C. Lee and S. Lee, *Nanotechnology*, 2009, 075202.
13 S. A. Coe-Sullivan, Ph.D. thesis, Massachusetts Institute of Technology, 2005.
14 P. O. Anikeeva, J. E. Halpert, M. G. Bawendi and V. Bulović, *Nano Lett.*, 2007, **7**, 2196–2200.
15 Y. Li, A. Rizzo, R. Cingolani and G. Gigli, *Adv. Mater.*, 2006, **18**, 2545–2548.
16 J. S. Steckel, P. Snee, S. Coe-Sullivan, J. P. Zimmer, J. E. Halpert, P. Anikeeva, L. A. Kim, V. Bulović and M. G. Bawendi, *Angew. Chem., Int. Ed.*, 2006, **45**, 5796–5799.
17 W. Y. Ji, P. T. Jing and J. L. Zhao, *J. Mater. Chem. C*, 2013, **1**, 470–476.
18 K. T. Shimizu, W. K. Woo, B. R. Fisher, H. J. Eisler and M. G. Bawendi, *Phys. Rev. Lett.*, 2002, **89**, 117401.
19 J. H. Kwak, W. K. Bae, D. G. Lee, I. Park, J. H. Lim, M. J. Park, H. D. Cho, H. J. Woo, D. Y. Yoon, K. H. Char, S. H. Lee and C. H. Lee, *Nano Lett.*, 2012, **12**, 2362–2366.
20 The EL spectraunder different voltages are not shown here. Instead, only the EL spectra at 7.0 V are shown in order to clearly identify the curves in Fig. 3b. The EL spectra from 4.5 V to 8.0 V are almost the same except for a neglectable red shift.
21 T. Y. Zhang, M. Liu, T. Li, J. Ma, D. L. Liu, W. F. Xie, C. L. Wu, S. W. Liu, S. C. Yeh and C. T. Chen, *J. Phys. Chem. C*, 2011, **115**, 2428–2432.
22 T. H. Kim, K. S. Cho, E. K. Lee, S. J. Lee, J. Chae, J. W. Kim, D. H. Kim, J. Y. Kwon, G. Amaratunga, S. Y. Lee, B. L. Choi, Y. Kuk, J. M. Kim and K. Kim, *Nat. Photonics*, 2011, **5**, 176–182.
23 Z. W. Liu, M. G. Helander, Z. B. Wang and Z. H. Lu, *J. Phys. Chem.*, 2010, **114**, 16746–16749.
24 J. Meyer, S. Hamwi, M. Kröger, W. Kowalsky, T. Riedl and A. Kahn, *Adv. Mater.*, 2012, **24**, 5408–5427.
25 J. R. Lakowicz, *Principles of Fluorescence Spectroscopy*, Springer, Berlin, Heidelberg, 3rd edn, 2006, pp. 443–527.
26 A. A. Lutich, G. X. Jiang, A. S. Susha, A. L. Rogach, F. D. Stefani and J. Feldmann, *Nano Lett.*, 2009, **9**, 2636–2640.
27 S. Coe-Sullivan, J. S. Steckel, L. A. Kim, M. G. Bawendi and V. Bulović, *Proc. SPIE–Int. Soc. Opt. Eng.*, 2006, **5739**, 108–115.

